

## PAPER



Cite this: *Soft Matter*, 2017,  
13, 2781

## Phase behavior of colloid–polymer depletion mixtures with unary or binary depletants†

Nayoung Park and Jacinta C. Conrad \*

Adding depletants to a colloidal suspension induces an attractive interparticle interaction that can be tuned to obtain desired structures or to probe phase behavior. When the depletant is not uniform in size, however, both the range and strength of the attraction become difficult to predict and hence control. We investigated the effects of depletant bidispersity on the non-equilibrium phase behavior of colloid–polymer mixtures. We added unary or binary mixtures of polystyrene as the depletant to suspensions of charged poly(methyl methacrylate) particles. The structure and dynamics of the particles were compared over three sets of samples with various mixtures of two different polystyrenes whose size varied by an order of magnitude. The structure and dynamics were nearly independent of depletant dispersity if the polymer concentration was represented as a sum of normalized concentrations of each species. Near the transition region between a fluid of clusters and an interconnected gel at intermediate volume fractions, partitioning of polymers in a binary mixture into colloid-rich and polymer-rich phase leads to a slightly different gelation pathway.

Received 30th December 2016,  
Accepted 18th March 2017

DOI: 10.1039/c6sm02891h

rsc.li/soft-matter-journal

### Introduction

Non-adsorbing macromolecules or nanoparticles induce attractive depletion interactions between microscale particles. Because both the strength and range of the attraction are readily tuned by the concentration and size of depletant, respectively,<sup>1–4</sup> mixtures of colloidal particles and depletants are commonly used to develop fundamental understanding of the effect of attractions on glass,<sup>5,6</sup> crystal,<sup>7,8</sup> and other phase transitions.<sup>3,9–13</sup> In industrial applications, depletion interactions induced by polymers added in storage or preparation may generate either desired structures<sup>14</sup> or deleterious aggregation<sup>15</sup> in products. In biology, crowding within cells affects the diffusion of macromolecules, and thereby alters reaction dynamics, macrostructure assembly, and protein folding.<sup>16–19</sup> Recent studies suggest that depletion interactions arising from small crowders may be one of the factors affecting intracellular diffusion.<sup>20,21</sup> In each of these settings, dispersity in the size of depletants changes the range and strength of the attraction, thereby altering the phase behavior of mixtures, the

stability of industrial products, or the diffusion of macromolecules within cells. Hence fundamental understanding of the effects of depletant size dispersity is expected to provide insight into and improve control over a range of industrial and biological processes.

Mixtures of uniformly disperse colloids and polymers are widely used to study equilibrium and non-equilibrium phase behavior in theory and experiment. For example, earlier theoretical studies found that adding short-ranged attractions to suspensions of particles with hard-sphere repulsions expanded the region of fluid-crystal coexistence, whereas adding longer-ranged attractions resulted in fluid–fluid phase separation.<sup>3,12</sup> In addition to these equilibrium phase transitions, experimental studies of depletion mixtures identified a variety of non-equilibrium phases, including clusters, gels, and glasses.<sup>9–11,13,22,23</sup> Most existing studies of phase behavior in depletion mixtures treated both particle and depletant as uniformly dispersed in size. Studies using theory/simulation<sup>24–27</sup> and experiment<sup>24,27–31</sup> probing the effects of particle size dispersity reported appearance of new phases or shifts in the phase boundaries with concomitant fractionation of particles by size. Although fewer in number, the extant studies exploring depletant size dispersity also tantalizingly hint at significant changes in the phase behavior of depletion mixtures. As one example, the concentration of polymer required to induce flocculation experimentally shifted by an order of magnitude from theoretical expectations when polymers with large dispersity were employed as the depletant.<sup>32,33</sup>

Systematic studies on the effect of depletant dispersity, however, report widely varying effects and hence are inconclusive. Theory and simulation studies, in which dispersity is readily

Department of Chemical and Biomolecular Engineering, University of Houston, Houston, TX 77204-4004, USA. E-mail: jconrad@uh.edu

† Electronic supplementary information (ESI) available: The ESI contains six figures: Fig. S1 (viscosity as a function of polymer concentration); Fig. S2 ( $g(r)$  and MSD for U6k samples); Fig. S3 (coordination number as a function of correlation length and  $\phi$ ), Fig. S4 (coordination number as a function of polymer concentration normalized by  $C_{p,exp}^*$  and  $\phi$ ), Fig. S5 (coordination number as a function of larger polymer concentration and  $\phi$ ), Fig. S6 (fraction of clusters as a function of cluster size for  $\phi = 0.25$ ), and Fig. S7 ( $g(r)$  of  $\phi \approx 0.01$  with screened Coulomb equation fit to data, with associated discussion). See DOI: 10.1039/c6sm02891h

tuned, have reported that increasing the dispersity of depletants: (1) increased both the range and strength of the attraction,<sup>34,35</sup> thereby lowering the concentration of depletant needed for phase separation;<sup>36,37</sup> (2) decreased the strength of attraction for constant depletant volume fraction;<sup>38,39</sup> or (3) negligibly affected the strength<sup>40,41</sup> and range<sup>40</sup> of depletion attractions. Similarly, contrasting experimental results suggest that the effects of polymer dispersity on interactions and phase behavior remain incompletely understood. Direct measurements of the force between a particle and a flat surface in a disperse polymer solution, for example, suggested that the smaller polymer in a mixture dominated the range of interaction,<sup>42</sup> or that knowledge of the whole distribution of polymer size was required to predict the attraction.<sup>43</sup> Likewise, contrasting effects of polymer size dispersity on non-equilibrium flocculation and gelation have been reported. Experiments using binary mixtures of polymers as depletant indicated that either the larger or smaller polymer could dominate flocculation, depending on the order in which polymers were added.<sup>44</sup> Later experimental studies<sup>45,46</sup> of gelation and flocculation, however, concluded that the larger polymer in mixtures controlled the phase behavior. Thus, understanding of the effects of polymer dispersity on non-equilibrium phase behavior remains limited and is the focus of this study.

Here, we show that the phase behavior of suspensions of charged colloidal particles containing dilute or semi-dilute unary or binary mixtures of polymer can be superimposed on a single phase diagram using an effective polymer concentration,  $C_{p,N}$  (the sum of the individual concentrations of polymers in a mixture, each normalized by their respective overlap concentrations). We varied the size of the polymer over one order of magnitude and characterized the structure and dynamics of the resulting colloid-polymer mixtures using confocal microscopy. Structural and dynamic metrics were nearly independent of depletant size or dispersity when the concentration of the polymer mixture was represented as a sum of normalized concentrations of each species, suggesting that the phase behavior in a mixture of polymers of different sizes can be predicted from the phase behavior of uniformly disperse polymers; disparities in these metrics occurred only near the transition between distinct phases. The normalized polymer concentration,  $C_{p,N}$ , was better able to collapse the phase behavior than the correlation length even in the semi-dilute regime of the polymer, indicating that both sizes of polymer contributed to the effective interparticle interaction.

## Materials and methods

### Sample preparation

Suspensions of poly(methyl methacrylate) particles (PMMA) were prepared at volume fractions of  $\phi = 0.05$ – $0.45$  with various concentrations and sizes of polystyrene (PS) polymers as depletants. We synthesized sterically stabilized PMMA particles following established protocols.<sup>47,48</sup> The average hydrodynamic radius of the particles was 990 nm and their polydispersity was 9%, as determined using dynamic light scattering. For imaging with

**Table 1** Summary of molecular weight ( $M_w$ ) and radius of gyration ( $R_g$ ) of the polystyrene polymers used in this study. The values of  $M_w$  and  $M_w/M_n$  are obtained from the vendor; the radius of gyration  $R_g$  was determined from intrinsic viscosity measurements

$M_w$ [Da]	$M_w/M_n$	Vendor	$R_g$ [nm]
6400	1.05	Scientific polymers	$2.8 \pm 0.1$
328 900	1.02	Agilent	$2.3 \pm 1$

the confocal microscope, particles were fluorescently labeled with Rhodamine B (Sigma Aldrich)<sup>49</sup> and dried for storage.

Each 0.5 mL sample was prepared by gravimetrically mixing pure solvent with stock suspensions/solutions of each component (particles, PS, and salt) in the solvent. The solvent was a mixture of cyclohexyl bromide (83.5 (w/w)%) and decahydro-naphthalene (16.5 (w/w)%), formulated to nearly match the refractive index and density of the particles. To prepare samples with particle volume fractions  $\phi \lesssim 0.25$ , a  $\phi = 0.48$  PMMA stock was diluted into each sample; to prepare samples with particle volume fractions  $\phi \gtrsim 0.25$ , dry PMMA particles were added directly to samples. We verified that both methods led to similar particle structure and dynamics. A stock tetrabutyl-(ammonium chloride) salt (TBAC) solution was added to each sample to a final concentration of 1.5 mM to partially screen charges on the particles.<sup>50,51</sup> The final TBAC concentration in solution—approximately 5  $\mu\text{M}$ —was much lower than the added concentration, due to the low degree of dissociation and solubility of TBAC in these solvent mixtures.<sup>50</sup> Stock solutions of two different PS polymers were prepared; the molecular weight ( $M_w$ , reported by the manufacturer) and radius of gyration ( $R_g$ , calculated from the measured intrinsic viscosity) of each polymer are given in Table 1. To vary the depletant dispersity and the attraction strength and range, we added one or two of the PS stock solutions to each sample. All PS used for this study induced short-ranged attractions, with  $R_g/a < 0.05$ , and the final concentration of PS in the free volume<sup>3,9</sup> was calculated using a concentration-dependent depletion layer thickness.<sup>4</sup>

Vials containing all components of a desired sample were tumbled and rolled to thoroughly mix the contents, and left on the roller until imaging. Most experiments were performed within 10 days of sample preparation, but all samples were imaged within 29 days of preparation. We verified that the dynamics and structure did not change with sample age over this period by comparing images acquired of samples past 10 days from preparation to those acquired at an earlier time point.

### Viscosity of PS solutions

We measured the viscosity of PS solutions at 20 °C using a Discovery Hybrid Rheometer (DHR-2, TA Instruments) and a Couette geometry with bob length of 42 mm. The viscosity at  $10 \text{ s}^{-1}$  for solutions at various  $C_p/C_p^*$  and  $M_w$  of PS collapsed onto a single curve with a quadratic dependence of viscosity on  $C_p/C_p^*$  and the y-intercept fixed at the solvent viscosity (Fig. S1, ESI†). Explicitly, we determined  $C_p^*$  for each of our samples by measuring the intrinsic viscosity and applying the relation  $C_p^*[\eta] \sim 1$ .

The quadratic fit to the data,  $\eta = \eta_s + 1.88c[\eta] + 1.39c^2[\eta]^2$ , agrees with the Huggins equation within fitting errors. This quadratic fit to the data was used to estimate the background viscosity for each sample.

### Imaging and tracking of particles

Approximately 100  $\mu\text{L}$  of each sample was sealed in a chamber fabricated from glass cover slides using UV-curable adhesive (Norland Optical). We imaged samples using a point-scanning confocal microscope, VT Eye (Visitech, Sunderland, U.K.) that was connected to an inverted microscope (Leica DMI 4000, Leica Microsystems, Buffalo Grove, IL) equipped with a  $63\times$  (N.A. 1.4) oil-immersion objective. Imaging began approximately 30 minutes after each sample was loaded into its chamber. To capture 3-D z-stacks of images, we rapidly acquired 2-D images (at 18.6 frames per second (fps),  $7.1 \text{ pixels } \mu\text{m}^{-1}$ ) that were spaced vertically by  $\Delta z = 0.1 \text{ } \mu\text{m}$  at heights from  $z = 25 \text{ } \mu\text{m}$  to  $65 \text{ } \mu\text{m}$  above the bottom coverslip. To generate sufficient statistics for quantitative structural measurements, at least nine z-stacks were acquired for  $\phi = 0.05$  samples and at least three z-stacks were acquired for  $\phi = 0.15$  samples; at higher volume fractions (*i.e.* for  $\phi \gtrsim 0.25$ ), one or two z-stacks were acquired for each sample. To characterize the dynamics of the particles, 2-D time series of images were captured at approximately 11 fps ( $6.3 \text{ pixels } \mu\text{m}^{-1}$ ) at a depth of  $30 \text{ } \mu\text{m}$  above the bottom coverslip.

We located the centers of the particles in 3-D in each z-stack using algorithms written in IDL.<sup>52</sup> The resolution of the particle centers was about 40 nm in the  $x$ - $y$  plane and about 200 nm in  $z$ , as determined from the mean-squared displacement (MSD) of stationary particles. We removed from the analysis any particles that were within about  $4 \text{ } \mu\text{m}$  of the edge in the  $x$ - $y$  plane and within  $1 \text{ } \mu\text{m}$  from the top and bottom. From the positions of the particle centers, we calculated the 3-D radial distribution function  $g(r) = n(r)/(\rho 4\pi r^2 dr)$ , where  $r$  is the distance from the center of particle,  $dr$  is the bin size,  $n$  is the number of particles in the shell between  $r$  and  $r + dr$ , and  $\rho$  is the bulk density of particles.

Using algorithms written in MATLAB, we located particle centers in 2-D in the time series of images and then tracked the particles over time.<sup>53</sup> To characterize the particle dynamics, we calculated the ensemble-averaged MSD, corrected for linear drift in the particle positions as  $\text{MSD} = \langle (x(t + \tau) - x(t))^2 \rangle$ , where  $x$  is the position of the particle,  $t$  is instantaneous time,  $\tau$  is the delay time, and the brackets represent averages over ensemble and time.

## Results and discussion

### Signatures of polymer-induced structure and dynamics

We first examined metrics for the structure and dynamics of the PMMA particles in the absence of polymer-mediated attractions. While PMMA particles are often used to model hard spheres, they may become charged during synthesis, when suspended in cyclohexyl bromide solvent, or with addition of salt.<sup>50,51</sup> In our

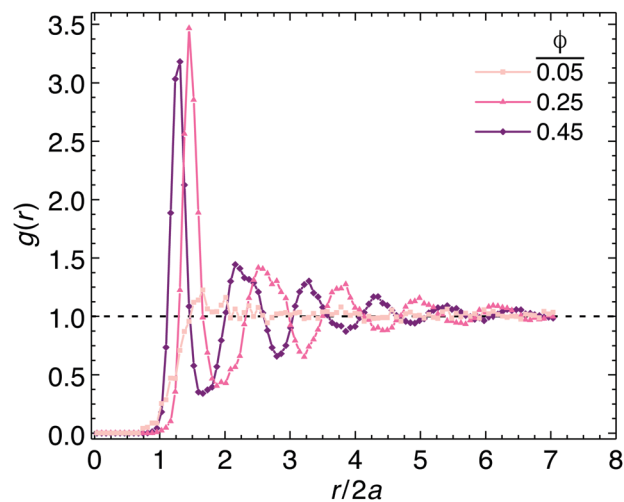


Fig. 1 Radial distribution function  $g(r)$  as a function of normalized radial distance  $r/2a$  for suspensions of PMMA without added polymer. The dashed line indicates the limiting value of  $g(r)$  at large  $r$  ( $g(r) = 1$ ).

experiments, the structure of the PMMA particles in suspensions without added depletant indicated that the particles were charged. The radial distribution function  $g(r)$  for the  $\phi = 0.05$  suspension increased sharply at a separation corresponding to the particle diameter ( $r/2a = 1$ ) but the first peak was shifted to  $r/2a = 1.7$ , indicating that particles exhibited long-range repulsive interactions (Fig. 1). Furthermore, the position of the first maximum of  $g(r)$ , one measure of the average separation between particles, shifted to lower values as the particle volume fraction  $\phi$  was increased from 0.25 to 0.45, as expected for suspensions of charged particles. The zeta potential and Debye length  $\kappa^{-1}$  were estimated to be  $-4.4 \text{ mV}$  and  $480 \text{ nm}$ , respectively, using a screened Coulomb potential fitted to the inter-particle potential estimated from  $g(r)$  measured at  $\phi \approx 0.01$  (Section SI2 in the ESI<sup>†</sup>). The samples did not crystallize because the polydispersity of our particles was at or above the values where crystallization is observed.<sup>54–56</sup>

Likewise, changes in dynamics with  $\phi$  as quantified by the ensemble-averaged one-dimensional MSD also indicated that the particles were charged. At  $\phi = 0.05$ , the MSD scaled with lag time as a power-law with exponent 1, *i.e.*  $\text{MSD} \sim \tau^1$ , consistent with Brownian diffusion; the experimentally-determined MSD closely agreed with that predicted from the Stokes–Einstein equation for a particle of the same size suspended in the same background viscosity as our samples (solid line in Fig. 2). The slight variation from the Stokes–Einstein estimate,  $D_{\text{SE}} = k_{\text{B}}T/6\pi\eta a$ , at short times was quantitatively accounted for by hydrodynamic interactions, which reduce the self-diffusion coefficient to  $D(\phi) \approx 0.92D_{\text{SE}}$  at this  $\phi$ .<sup>57</sup> At volume fractions  $\phi \geq 0.25$ , however, the MSD was nearly constant at long lag times. The plateau in MSD signals caging of the particles by neighbors,<sup>58–60</sup> and is usually expected at significantly higher volume fractions in hard spheres. Hence this result suggested that the effective volume fraction in our suspensions was higher than the actual particle volume fraction due to the long-range electrostatic repulsions between particles. As the volume fraction was further

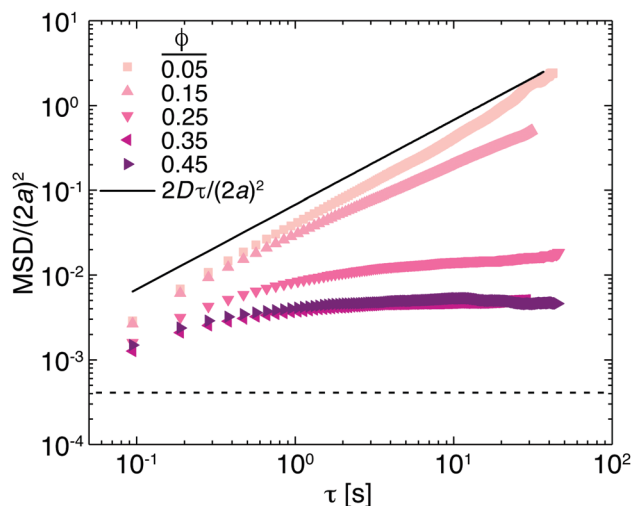


Fig. 2 Normalized mean-squared displacement  $\text{MSD}/(2a)^2$  as a function of delay time  $\tau$  for PMMA suspensions with no added polymer. The solid line indicates the MSD calculated from the Stokes–Einstein equation. The dashed line indicates the resolution of the tracking algorithm.

increased above  $\phi = 0.25$  the height of the plateau decreased, suggesting that the particles were increasingly caged. The MSDs measured at the two highest  $\phi$  were equal, indicating that the

average cage size did not significantly change at these higher volume fractions. The cage size estimated from the limiting plateau MSD value, 140 nm, was of the same order of magnitude as the estimated Debye length (480 nm, as described in the ESI†), consistent with strong caging due to the electrostatic repulsions.

Adding PS polymers to induce attractions between the PMMA particles led to changes in both the structure and dynamics of the particles. We first examined the behavior of samples with added polymers of uniform molecular weight (328.9 kDa) as a function of depletant concentration and particle volume fraction. As PS concentration increased, the height of the  $g(r)$  maximum corresponding to the average interparticle separation decreased; concomitantly, a new local maximum appeared at a lower separation corresponding to the average particle diameter ( $r/2a = 1$ ) (Fig. 3a–c). The finite width of this contact peak nearly quantitatively reflected both the particle size dispersity and errors in locating the centers of particles. The appearance of the contact peak and its increase in height with PS concentration indicated that a significant fraction of particles was in near-contact with their neighbors, consistent with the formation of multiparticle structures such as clusters or gels.

Similarly, the dynamics of the particles also evolved with increasing PS concentration (Fig. 3d–f). Increasing the PS concentration

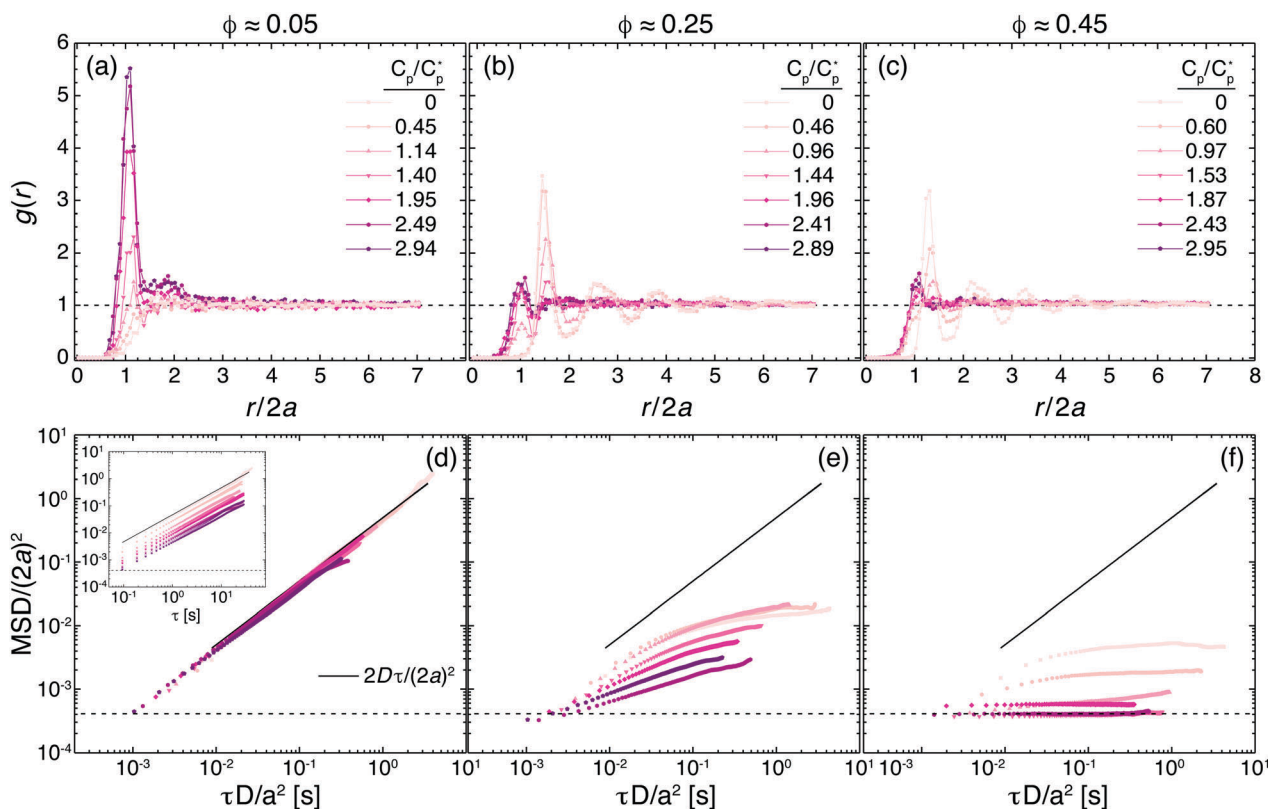


Fig. 3 (a–c) Radial distribution function  $g(r)$  as a function of normalized radial distance  $r/2a$  and (d–f) normalized mean squared displacement  $\text{MSD}/(2a)^2$  as a function of non-dimensionalized delay time  $\tau D/a^2$ , for PMMA suspensions with various concentrations of 328.9 kDa PS and particle volume fractions of (a and d)  $\phi \approx 0.05$ , (b and e)  $\phi \approx 0.25$ , or (c and f)  $\phi \approx 0.45$ . The dashed lines in (a–c) indicate the limiting value of  $g(r)$  at large  $r$ . The inset in (d) shows  $\text{MSD}/(2a)^2$  as a function of delay time  $\tau$  for suspensions with volume fraction of  $\phi \approx 0.05$  without the viscosity correction. The dashed lines in (d–f) indicate the resolution of the measurement  $\epsilon^2/(2a)^2$ .

strengthened the depletion attraction but also increased the background solvent viscosity; both factors caused the diffusivity to decrease. To isolate the change in the MSD due to attractive interactions, the delay time was non-dimensionalized using the ratio of the Stokes–Einstein diffusion coefficient to the square of the radius of the particles,  $D/a^2$ . This non-dimensionalization shifted the MSD of samples with added polymers to lower delay times. At the lowest particle volume fraction ( $\phi = 0.05$ ), the MSD curves acquired at various concentrations of PS collapsed onto a single curve as a function of the viscosity-corrected delay time (Fig. 3d), indicating that the slowing of dynamics (Fig. 3d inset) was solely due to the increase in viscosity. We did not observe dynamics indicative of a depletion layer,<sup>61–63</sup> likely because the range of depletion was less than 5% of the particle size in all samples. At higher particle volume fractions (e.g.  $\phi = 0.25, 0.45$ ), the MSD decreased with increasing PS concentration at a fixed non-dimensional lag time (Fig. 3e and f); these changes indicated that the dynamics slowed due to the increase in the strength of the attractive interactions between particles. At  $\phi = 0.45$ , the magnitude of the MSD for samples with the highest concentrations of polymer was approximately equal to the tracking resolution  $\varepsilon^2/(2a)^2$ , indicating that the particles were effectively arrested over the duration of the experiments. (Similar  $g(r)$  and MSD data for samples with only the lower molecular weight PS (6.4 kDa) are shown in Fig. S2, ESI†).

To investigate the effect of depletant dispersity on structure and dynamics, we examined  $g(r)$  and MSD for PMMA suspensions containing PS of two different sizes (Fig. 4, 6.40 kDa and 328.9 kDa). Like suspensions with depletants of uniform size, at sufficiently high total PS concentration  $g(r)$  exhibited a contact peak and the long-time MSD decreased. These changes in  $g(r)$  and MSD, however, occurred at a lower critical concentration of the larger PS (328.9 kDa) in suspensions with binary polymer mixtures than for suspensions with only the 328.9 kDa PS. In samples containing only 328.9 kDa PS, a normalized polymer concentration  $C_p/C_p^* \geq 0.96$  was required at  $\phi = 0.25$  to obtain a contact peak in  $g(r)$  and a decrease in MSD; in samples containing both 6.40 kDa and 328.9 kDa PS,  $C_p/C_p^* \geq 0.53$  of 328.9 kDa PS was required at the same particle volume fraction to obtain a contact peak in  $g(r)$ . The decrease in critical  $C_p/C_p^*$  of the larger PS indicated that the smaller polymer in the binary mixture also contributed to the attractive interaction – even though  $R_g$  of the 6.40 kDa polymer was only about 0.3% of the PMMA particle radius.

#### Comparison of unary and binary mixtures: metrics and normalization

To probe how polymers of different size contribute to the phase behavior of PMMA particles, we compared the structure and dynamics across sets of samples containing small, large, or

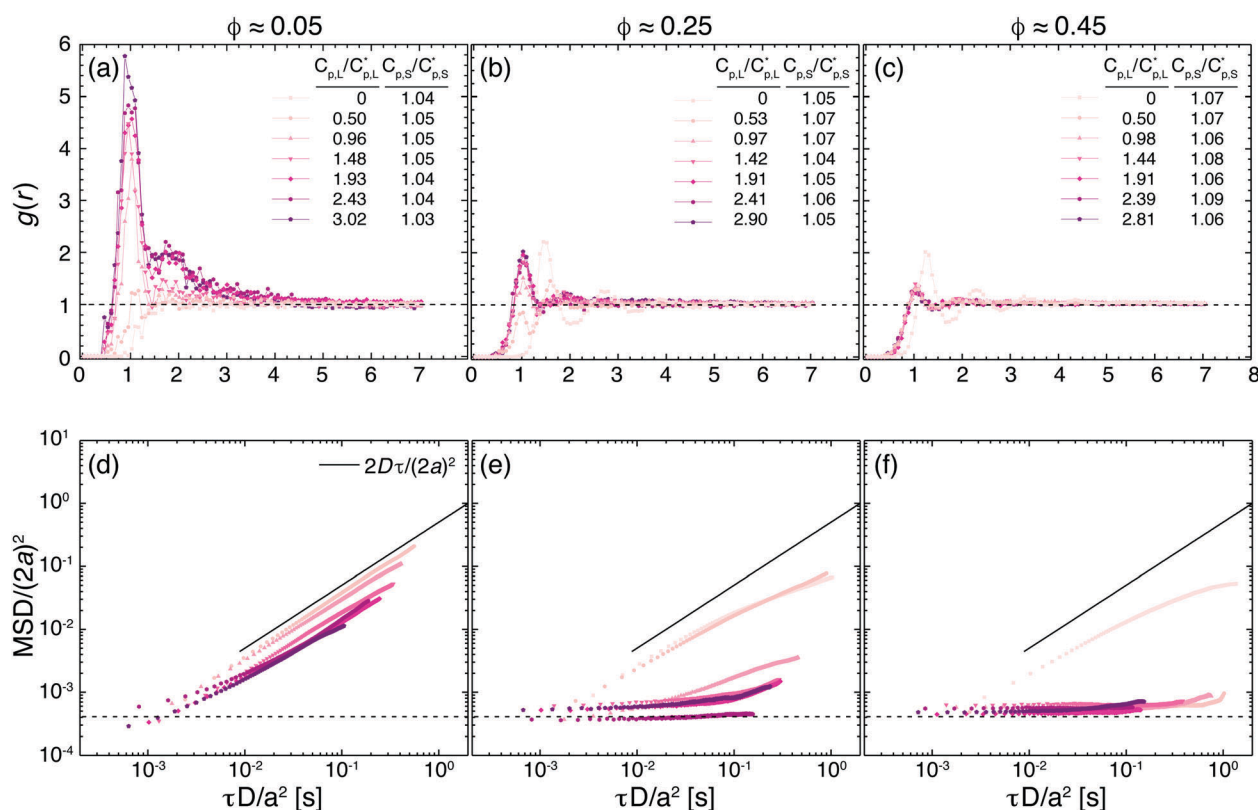


**Fig. 4** (a–c) Radial distribution function  $g(r)$  as a function of normalized radial distance  $r/2a$  and (d–f) normalized mean squared displacement  $\text{MSD}/(2a)^2$  as a function of non-dimensionalized delay time  $\tau D/a^2$ , for PMMA suspensions with various concentrations of 328.9 kDa PS ( $C_{p,L}/C_{p,L}^*$ ) and fixed concentration of 6400 Da PS ( $C_{p,S}/C_{p,S}^*$ ). The particle volume fractions are (a and d)  $\phi \approx 0.05$ , (b and e)  $\phi \approx 0.25$ , or (c and f)  $\phi \approx 0.45$ . The dashed lines in (a–c) indicate the limiting value of  $g(r)$  at large  $r$ ; the dashed lines in (d–f) indicate the resolution of the tracking algorithm  $\varepsilon^2/(2a)^2$ .

**Table 2** Depletant dispersity (unary/binary) and  $M_w$  of the PS depletants added to each sample set

Sample set	Symbol in figures	Unary/binary	PS $M_w$
U6k	$\Delta$	Unary	6.40 kDa
U300k	$\square$	Unary	328.9 kDa
B300k	$\blacksquare$	Binary	328.9 kDa + 125 mg mL <sup>-1</sup> 6.40 kDa

both PS (Table 2). Determining the effects of depletant size and dispersity on the phase behavior of the particles across the different sets of samples required quantitative measures for particle structure and dynamics. As metrics for structure, we calculated the coordination number  $N$  and the particle density fluctuations  $\Delta\rho_{10}$  over boxes of size  $(10\ \mu\text{m})^3$ .  $N$  is a measure of the average number of particles whose centers fall within the first coordination shell and hence are in near-contact. Larger values of  $N$  indicated that, on average, a particle was in close contact with more surrounding particles; hence increasing the particle volume fraction was expected to increase the coordination number. At constant particle volume fraction, higher values of  $N$  are consistent with particle aggregation. To calculate coordination number, we determined the location of the first minimum  $r_{\min}$  in  $g(r)$  for those samples whose pair correlation functions exhibited both a contact peak and an average-separation peak. Subsequently,  $g(r)$  was numerically integrated to the average  $r_{\min}$  to obtain  $N = \int_0^{r_{\min}} 4\pi r^2 \rho g(r) dr$ .

In addition to the local structure, we quantified the long-range structural heterogeneity *via* the particle density fluctuations  $\Delta\rho_{10}$  over boxes of side length  $10\ \mu\text{m}$ .<sup>64,65</sup> The  $\Delta\rho_{10}$  metric was calculated *via*  $\Delta\rho_{10} = \frac{\langle N_p^2 \rangle - \langle N_p \rangle^2}{\langle N_p \rangle}$ , where  $N_p$  is the number of particles in each box. If particles formed large voids during clustering and gelation, the structural heterogeneity was expected to increase above the hard-sphere value of 0.21.<sup>64,66</sup> Indeed, depletion gels were previously shown to exhibit a local maximum in heterogeneity as a function of the strength of the attraction.<sup>64</sup>

As a metric for dynamics, we examined the value of the MSD at a constant delay time of 10 s,  $\text{MSD}_{10\text{s}}$ ; most samples that exhibited a plateau in MSD reached it by this lag time. Changes in  $\text{MSD}_{10\text{s}}$  reflected changes in the structure and/or dynamics of the suspension. For example, increasing the volume fraction of the particles in the absence of depletant decreased  $\text{MSD}_{10\text{s}}$ , reflecting a decrease in the size of the cage to which particles were localized (Fig. 2). Increasing the polymer concentration at constant particle volume fraction also decreased  $\text{MSD}_{10\text{s}}$ , reflecting the slowing of particle dynamics with increasing viscosity or with formation of clusters and gels (Fig. 3 and 4d–f).

To quantitatively compare changes in structure across all sets of samples, we first examined the behavior of  $N$  as a function of normalized polymer concentration and particle volume fraction. The concentrations of polymers used in this study varied by over an order of magnitude across the different sample sets, requiring normalization of the polymer concentration for effective comparisons. Whereas the concentration of unary PS could be normalized by the overlap concentration of

the polymer, this normalization could not be applied directly to samples that contained binary mixtures of PS. We therefore examined several methods to normalize the polymer concentration and thereby compare across unary and binary polymer mixtures.

First, we compared the values of the structural metric  $N$  as a function of the polymer correlation length. The depletant concentration in most of our samples was above the overlap concentration, so that the polymer solutions were in the semi-dilute regime. In this concentration regime, the strength of the depletion attraction is inversely proportional to the correlation length  $\xi$ ,<sup>67,68</sup> the distance between polymer chains. Samples of similar  $\phi$  and  $\xi$  but different polymer dispersity, however, exhibited distinct structures (Fig. S3, ESI†). Because the correlation length was not able to uniformly describe the observed trends in structure across all sample sets, we posited that the size of the polymer coils affected the structure of the particles even when they were overlapping. To confirm this idea, we normalized the concentration of polymers in binary mixtures by the average overlap concentration  $C_{p,\text{exp}}^* = M_w/(4\pi R_{g,z}^3 N_A/3)$ ,<sup>69</sup> where  $R_{g,z}$  is the z-average radius of gyration of the polymer mixture, and compared the structural metric at similar locations in the  $(\phi, C_p/C_{p,\text{exp}}^*)$  plane. This normalization also failed to describe the trends in structure across the sample sets, confirming that the two sizes of PS in the binary mixtures induced depletion attractions as independent polymers, even in the semi-dilute regime (Fig. S4, ESI†). Finally, we examined the coordination number as a function of the larger polymer concentration (Fig. S5, ESI†). Again, the phase behavior was not captured by this concentration across all samples, indicating that the smaller polymer could not be neglected.

Although polymer physics suggests that  $\xi$  should describe the mixture of polymers, earlier theoretical<sup>34,36,37</sup> and experimental<sup>44,45</sup> studies on the effect of depletant dispersity on the phase behavior of colloids suggested that a single size (whether  $\xi$  or an average polymer size) was insufficient to describe depletion in highly disperse systems. Instead, knowledge of the depletant size distribution was required to understand the resulting phase behavior. As a simple way to account for the distribution of polymer sizes in our binary mixture, we represented the total PS concentration as a sum of the concentrations of each species in a mixture, normalized by their individual overlap concentrations:  $C_{p,N} = C_{p,L}/C_{p,L}^* + C_{p,S}/C_{p,S}^*$ , where  $C_{p,L}$  ( $C_{p,S}$ ) is the concentration of the larger (smaller) PS in a mixture, and  $C_{p,L}^*$  ( $C_{p,S}^*$ ) is the overlap concentration of the large (small) polymer. In the dilute regime of the polymer ( $C_p/C_p^* < 1$ ) the individual polymer coils do not overlap, and  $C_{p,N}$  approximately represents the volume fraction of polymer coils. In earlier theoretical work, the equilibrium phase behavior was shown to be independent of polymer dispersity in the dilute regime under this normalization.<sup>37,70</sup> In our experiments, however, the polymer concentration in most of the samples was in the semi-dilute regime ( $C_p/C_p^* > 1$ ), where  $C_{p,N}$  does not correspond to the volume fraction because the polymer coils overlap. Instead,  $C_{p,N}$  sums the individual contributions of both polymers in the mixture. Nonetheless, we found that samples with similar

values of  $C_{p,N}$  exhibited very similar values of the coordination number across a broad range of polymer sizes and dispersity.

### Structural comparisons

To compare the local structure of unary and binary mixtures, we examined the behavior of  $N$  as a function of the normalized polymer concentration  $C_{p,N}$  and particle volume fraction  $\phi$ . We found that  $N$  for all three sample sets collapsed onto a single phase diagram, independent of depletant size or dispersity (Fig. 5a). This agreement suggested that the local structure of the particles depended on the normalized concentration of polymer and not on its dispersity. Further,  $N$  did not change significantly with increasing  $C_{p,N}$  until the polymer solution was in the semi-dilute regime for the three sets of samples. Although phase transitions are expected at much lower polymer concentrations for hard-spheres,<sup>3,9,23</sup> both theoretical<sup>71,72</sup> and experimental<sup>73</sup> studies showed that increasing the Debye length can shift the phase boundaries to significantly higher concentrations of depletant. In our system, the Debye length estimated from  $g(r)$ , 480 nm, was much larger than the radii of gyration of the two polymers, 2.8 nm and 23 nm; it was therefore reasonable that no phase transition was observed in our samples at low polymer concentrations.

To compare structure of particles on larger length scales, we also examined the behavior of  $\Delta\rho_{10}$  over boxes of size  $(10\ \mu\text{m})^3$  as a function of  $C_{p,N}$  and  $\phi$ . The  $\Delta\rho_{10}$  metric also agreed closely for all three sample sets as a function of normalized polymer concentration across nearly all of the  $(\phi, C_{p,N})$  parameter space, indicating that the long-range structure of the samples was also independent of polymer dispersity (Fig. 5b). Consistent with the two metrics, micrographs of samples in sample sets U6k, U300k, and B300k revealed similar structures, irrespective of PS size and dispersity (Fig. 5c). The greatest disparity in large-scale structure revealed in the micrographs (between sample sets U300k and B300k at a volume fraction of  $\phi = 0.25$  and  $C_{p,N} \approx 2.5$ , Fig. 5c, sample a1) was consistent with the region of greatest disparity in the density fluctuations (Fig. 5b). To uncover the origin of these disparities, we examined the dependence of the density fluctuations for samples at fixed volume fractions as a function of  $C_{p,N}$ . Surprisingly, we did not observe a local maximum in  $\Delta\rho_{10}$  across the gelation transition seen in the micrographs, which was observed in an earlier study on a similar system;<sup>64</sup> the width of the maximum in that study, however, was smaller than the step size in  $C_{p,N}$  used here. At  $\phi = 0.25$  and  $C_{p,N}$  between 2.5–3, the binary sample exhibited an increase in  $\Delta\rho_{10}$ , which suggests formation of larger voids, and may signal a nearby structural transition (Fig. 6b); the corresponding unary samples, however, exhibited little change in  $\Delta\rho_{10}$  with  $C_{p,N}$ . These results suggested that the effects of polymer dispersity on structure may be most pronounced near transition boundaries.

To test the hypothesis that this discrepancy in structure arose due to an incipient transition, we closely investigated cluster formation for the three sample sets at  $\phi = 0.25$ . Many factors affect clustering and gelation for particles with short-ranged attractive and long-ranged repulsive interactions,

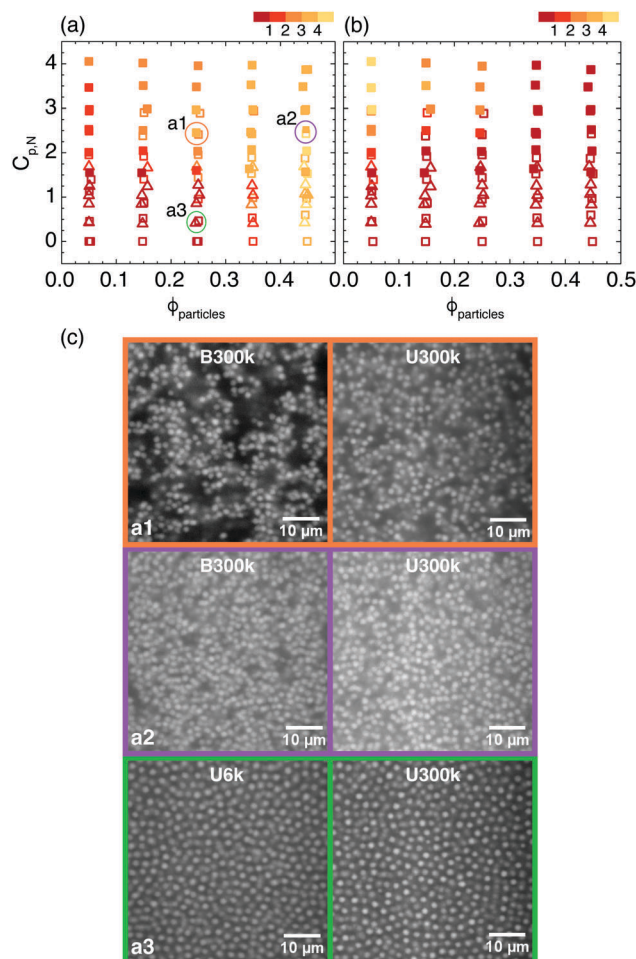


Fig. 5 Color representation of the (a) coordination number  $N$  and (b) density fluctuations over  $(10\ \mu\text{m})^3$   $\Delta\rho_{10}$  as a function of normalized polymer concentration  $C_{p,N} = C_{p,L}/C_{p,L}^* + C_{p,S}/C_{p,S}^*$  and particle volume fraction  $\phi$  for PMMA suspensions containing unary (open) and binary (closed) mixtures of PS of molecular weights 6.40 kDa and 328.9 kDa (sample sets U6k, U300k, and B300k). The colorbar indicates the values of  $N$  and  $\Delta\rho_{10}$ . Symbol key:  $\Delta$  U6k,  $\square$  U300k,  $\blacksquare$  B300k. (c) Confocal micrographs acquired at a height of  $z = 30\ \mu\text{m}$  above the bottom of the sample chamber for sample sets U6k, U300k, and B300k. The three rows of images represent samples with similar particle volume fraction  $\phi$  and normalized polymer concentration  $C_{p,N}$ .

including the balance between the strengths of the repulsive and attractive interactions, the range of the repulsive interactions, and the particle volume fraction.<sup>74–79</sup> As metrics to identify the onset of cluster formation, growth, and gelation, we calculated the fraction of particles in the measurement volume remaining as monomers and in the largest cluster; particles were defined to be in a cluster if their nearest neighbor was closer than  $r_{\text{min}}$ . Although all clustered samples must have a largest cluster, we found that samples formed an interconnected gel if a majority ( $\geq 50\%$ ) of the particles in the measurement volume were in the largest cluster. The combination of particle polydispersity and resolution of the tracking algorithm led to a large value of  $r_{\text{min}}$ , so that some monomeric particles were counted as clustered. Thus, the fraction of monomer was less

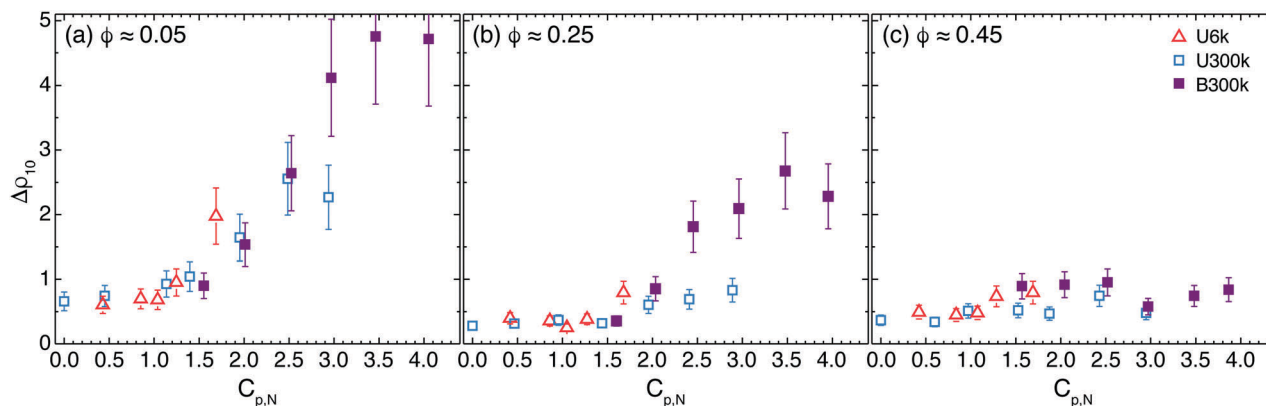


Fig. 6 Density fluctuations over boxes of size  $(10 \mu\text{m})^3$   $\Delta\rho_{10}$  as a function of normalized polymer concentration  $C_{p,N}$  for sample sets U6k, U300k and B300k. Particle volume fractions  $\phi$  are (a) 0.05, (b) 0.25, and (c) 0.45. The approximate sample-to-sample variability is represented as error bars.

than one for samples without added PS (Fig. 7a); in these samples, a vanishing fraction of particles were in the largest

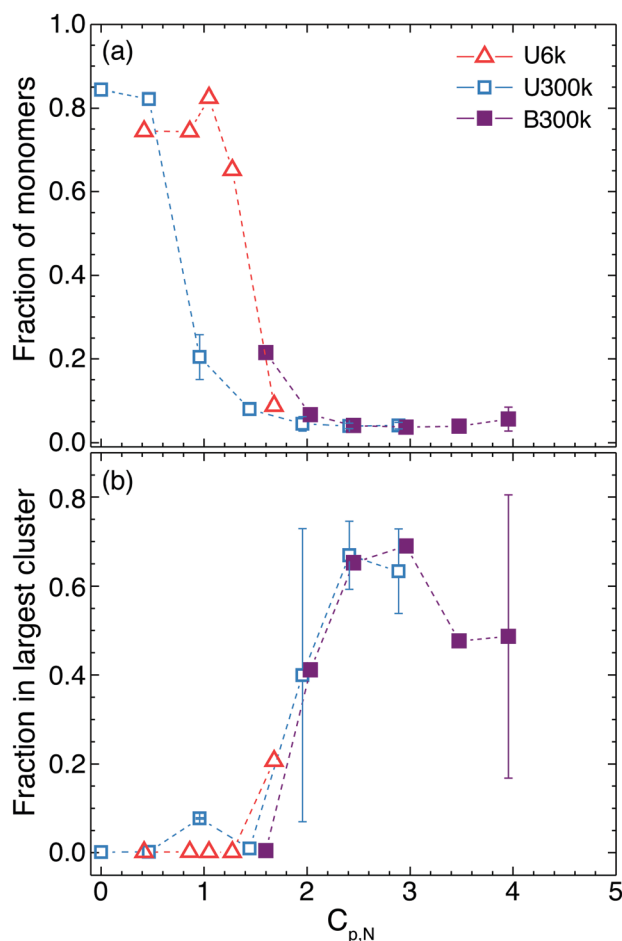


Fig. 7 (a) Fraction of particles in a sample volume that remain as monomers as a function of normalized polymer concentration  $C_{p,N}$  for samples at particle volume fraction  $\phi = 0.25$  in sample sets U6k, U300k, and B300k. (b) Fraction of particles in a sample volume in largest cluster as a function of  $C_{p,N}$  for samples shown in (a). The dashed lines are guides to the eye; the error bars represent measured sample-to-sample variability.

cluster, indicating that any apparent clusters remained small (Fig. 7b).

This analysis of clustering suggested that samples containing the small PS (U6k and B300k) may gel through a different pathway than samples without small PS (U300k). For the unary large-polymer sample series (U300k), the fraction of monomer decreased starting at  $C_{p,N} \sim 0.5$ , indicating the formation of small clusters. At this concentration, however, fewer than 10% of particles were in the largest cluster; only when the polymer concentration was increased above  $C_{p,N} \sim 1.5$  did the size of the largest cluster grow rapidly. This behavior suggested that formation of small disconnected clusters (at lower strengths of attraction) preceded gelation in this series of samples. By contrast, in samples containing the smaller PS (U6k and B300k), the concentration of polymer at the onset of cluster formation (signaled by the decrease in monomer fraction) nearly coincided with the onset of the increase in size of the largest cluster, near  $C_{p,N} \sim 1.2$ . This behavior suggested that particles in these samples formed a space-spanning network directly from monomers; here the presence of small polymer appeared to suppress the formation of many small clusters. The transition from monomers/clusters to gels occurred over normalized concentrations of  $C_{p,N} \sim 2-3$ , where the size of the largest cluster increased rapidly with PS concentration. This transition region corresponded with the region of discrepancy in structure reported in Fig. 5b, c and 6. Nonetheless, the final structure of the gels in all sample sets (at high polymer concentrations) was similar despite the different pathways to the gel.

To estimate the location of the gelation boundary, we also calculated the cluster size distribution at  $\phi = 0.25$ . Earlier studies showed that the size distribution of clusters approaches a power law at the gelation boundary.<sup>22,80</sup> From the behavior of the cluster fraction  $n(s)$  as a function of cluster size  $s$  for different samples, we estimated that gelation occurred near  $C_{p,N} \approx 1.4 \pm 0.2$  (Fig. S6, ESI†). All B300k samples studied here exhibited this power-law scaling, precluding the use of this method to determine the gelation boundary. Nonetheless, all samples in the three sets formed gels when  $C_{p,N} \geq 1.4$ , suggesting that these samples may have similar gelation boundaries.

For short-ranged attractions, the phase behavior is expected to be independent of the shape of the interaction potential and to depend only on the reduced second virial coefficient  $B_2$ , per the law of corresponding states.<sup>81</sup> Indeed, a careful comparison between experiment and simulation in a similar system confirmed that  $n(s)$  as a function of  $s$  depended only on  $B_2$ .<sup>22</sup> Here, our measurements are consistent with the expectation that the gelation boundaries should coincide for all three sets of samples.

### Dynamics

The dynamics of the particles in sample sets U300k and B300k, as quantified by  $\text{MSD}_{10\text{s}}$ , also largely collapsed onto a single diagram as a function of  $C_{\text{p,N}}$  and  $\phi$ , irrespective of polymer dispersity (Fig. 8). The  $\text{MSD}_{10\text{s}}$  of the sample set containing only the smallest PS (U6k), however, did not collapse on the same diagram as U300k and B300k, with the disparity between sample sets most pronounced between samples with  $\phi \geq 0.25$  and  $C_{\text{p,N}} \approx 1$ .

To investigate the origin of the disparity in dynamics, we examined the dependence of  $\text{MSD}_{10\text{s}}$  on  $C_{\text{p,N}}$  for  $\phi = 0.05, 0.25$ , and  $0.45$  (Fig. 9). For the samples containing large polymer (U300k and B300k),  $\text{MSD}_{10\text{s}}$  decreased approximately monotonically with  $C_{\text{p,N}}$ . In sharp contrast, the  $\text{MSD}_{10\text{s}}$  did not depend monotonically on normalized polymer concentration for the U6k samples at volume fractions  $\phi \geq 0.25$ ; instead,  $\text{MSD}_{10\text{s}}$  increased concomitant with PS concentration up to  $C_{\text{p,N}} = 1$ , then decreased as  $C_{\text{p,N}}$  was further increased. Non-monotonic behavior of the MSD with increasing polymer concentration was also observed in the MSD of U6k samples, shown as a function of  $\tau D/a^2$  in Fig. S2d–f (ESI<sup>†</sup>). This behavior was reminiscent of re-entrant melting, observed for hard-sphere

particles at higher volume fractions near or above that required for the glass transition.<sup>82–84</sup> We attributed this behavior to the high effective volume fraction in these samples, which resulted from the strongly repulsive interactions between the particles. To estimate the effects of the repulsions on the effective volume fraction, we estimated the Debye length ( $\kappa^{-1}$ ) to be approximately 480 nm (Section SI2 in the ESI<sup>†</sup>). Using an effective particle radius that accounted for the electrostatic repulsions, the effective volume fractions for  $\phi = 0.25$  and  $0.45$  were estimated to be 0.39 and 0.71, respectively. Given the high effective volume fractions, it was reasonable that weak to moderate short-ranged attractions could reduce the time scale required for particles to escape their cages.

This re-entrant melting behavior, due to the smaller PS, may also contribute to the shift in  $C_{\text{p,N}}$  in the onset of cluster formation for U6k and B300k. The increased mobility imparted by the presence of the small polymers may allow particles to remain monomeric up to higher  $C_{\text{p,N}}$ , thus shifting the formation of clusters to higher polymer concentrations. In our charged-sphere system, the melting behavior was only observed for the shorter polymer; in hard-sphere systems, however, re-entrant melting behavior was observed for larger polymer-colloid size ratios than that of our large polymer.<sup>5,82,83</sup> This comparison suggests that the (modest) disparities between unary and binary mixtures may become less pronounced, or even vanish entirely, if the size of the smallest polymer species exceeds the apparent cutoff for re-entrant effects.

### Role of polymer partitioning

Our measurements suggest that quantifying the polymer concentration as  $C_{\text{p,N}}$ , the sum of the individual contributions of each polymer in a binary mixture, led to close agreement of structure and dynamics between samples with unary and binary mixtures of depletants. This result indicates that both polymers in a binary mixture contribute to the depletion interaction. Earlier theoretical work on the equilibrium phase behavior of depletant systems with a binary mixture of depletants<sup>37</sup> and with polydisperse depletants<sup>36</sup> showed that the depletants partition by size into colloid-rich and polymer-rich phases. In these studies, the larger polymers were excluded from the colloid-rich phase.<sup>36</sup> This behavior was similar to another entropically-driven phenomenon: partitioning of bimodal polymers within porous media.<sup>85</sup> Theoretical analysis of this partitioning showed that the concentration of the smaller polymer in the pores could exceed its bulk concentration if the concentration of the larger polymer in the bulk was above its overlap concentration.<sup>85</sup> In that system, the extent of partitioning depended on the normalized concentrations of both species.

Polymer partitioning also has practical consequences for particle aggregation. As one example, the flocculation boundaries of silica particles in the presence of binary mixtures of polymers depended on the order in which the polymers were added to the suspension.<sup>44</sup> When both polymers were added simultaneously, the flocculation boundary coincided with that obtained when the smaller polymers were added first.

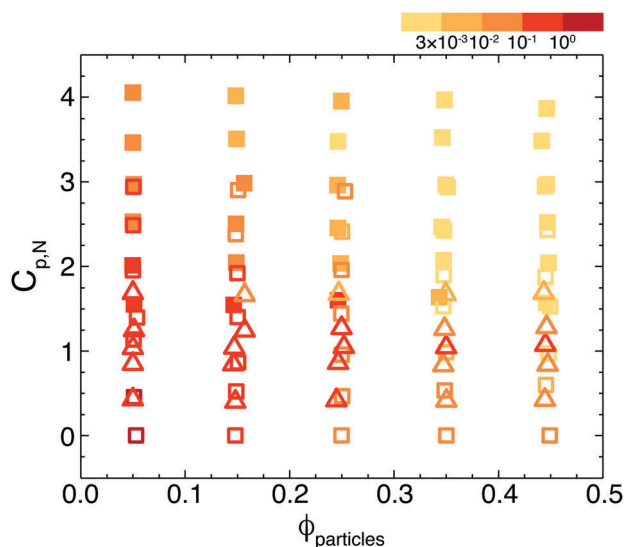


**Fig. 8** Color representation of the mean-squared displacement at a fixed time of 10 s,  $\text{MSD}_{10\text{s}}$ , as a function of normalized polymer concentration  $C_{\text{p,N}}$  and particle volume fraction  $\phi$  for PMMA suspensions containing unary (open) and binary (closed) mixtures of PS (sample sets U6k, U300k, and B300k). The colorbar indicates the value of  $\text{MSD}_{10\text{s}}$ . Symbol key:  $\Delta$  U6k,  $\square$  U300k,  $\blacksquare$  B300k.

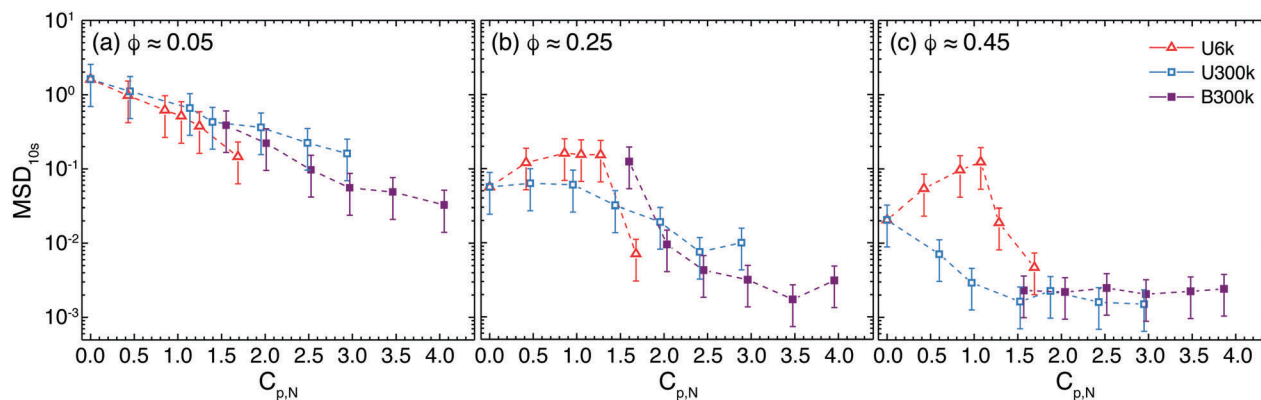


Fig. 9 Mean-squared displacement at a constant delay time of 10s,  $MSD_{10s}$ , as a function of normalized polymer concentration  $C_{p,N}$  for PMMA suspensions containing unary and binary mixtures of PS of molecular weights 6.40 kDa and 328.9 kDa at particle volume fractions of (a) 0.05, (b) 0.25, and (c) 0.45. The error bars represent approximate sample-to-sample variability.

This result suggested a physical picture in which the smaller polymers first caused particles to form “pseudoflocs,” from which the larger polymer was excluded by its size.<sup>44</sup> In that study, partitioning was proposed to increase the bulk concentration of the larger polymers, thereby increasing the strength of attraction between the silica particles. Later theoretical work<sup>37</sup> revealed that this partitioning of polymers by size occurred in equilibrium, with more distinct partitioning as the size ratio between the polymers increased.

Based on these earlier studies, we conjecture that our binary system (featuring an order of magnitude difference in the radius of the polymers) partitions into colloid-rich and polymer-rich phases. At the onset of cluster formation, we expect that the smaller polymer would be more concentrated in and around clusters than the larger polymers; the larger polymers would then increase the attraction strength between the clusters as their bulk concentration increased. Hence partitioning of polymers by size could explain the slight discrepancy in the structure and dynamics observed near the fluid-to-solid transition at  $\phi = 0.25$ . As gels formed, the exclusion of the larger polymer from the colloid-rich phase would increase its concentration in the bulk. The resulting increase in the osmotic pressure could push the gel network closer together to form more compact gels with larger void spaces and would explain the larger density fluctuations of the gels with binary mixtures than with unary depletants (*cf.* Fig. 6). Furthermore, the trends in cluster fraction in Fig. 7 suggest that gels in the binary mixture appeared to form directly from monomers; this pathway may arise from the increased attraction between any temporary clusters that form, due to the increase in bulk concentration of the larger polymer. Effects from polymer partitioning are expected to be most pronounced near flocculation boundaries at which large clusters appeared – and hence did not strongly affect the phase behavior at  $\phi = 0.05$  (which never formed gels) or at  $\phi = 0.45$  (which did not exhibit large void spaces). Indeed, the overall phase behavior was very similar in the three sample sets when the individual contributions of the polymers in the binary mixture were accounted for using  $C_{p,N}$ .

## Conclusions

We explored the effects of polymer dispersity on the non-equilibrium phase behavior of colloid–polymer depletion mixtures. The structure (quantified *via* coordination number  $N$  and density fluctuations  $\Delta\rho_{10}$ ) and dynamics (quantified *via*  $MSD_{10s}$ ) for samples with short-ranged attractions at similar values of the particle volume fraction  $\phi$  containing unary or binary polymer mixtures could be collapsed onto a single phase diagram as a function of a normalized polymer concentration  $C_{p,N}$ . The failure to obtain a single diagram using the polymer correlation length or the large-polymer concentration indicated that binary mixtures of PS could not be treated as homogeneous solutions; instead, both sizes of polymer contributed to the effective interaction. Deviations from this picture occurred in two cases: (i) close to the transition from a fluid of clusters to a gel, for which the pathway of gelation varied between sample sets; and (ii) in suspensions of moderate to high particle volume fractions containing only small polymers, which exhibited non-monotonic changes in dynamics reminiscent of re-entrant melting. These slight discrepancies were consistent with a physical picture in which the polymer partitioned into colloid-rich and polymer-rich phases, suggested by earlier theoretical work on binary polymer mixtures. Hence, if the smaller polymer were closer in size to the larger polymer in the binary mixture, the polymers would partition less and discrepancies would be less pronounced.

The inability of the correlation length to describe the phase behavior of particles in a binary mixture of polymers suggests that the full molecular weight distribution of the polymer must be known to calculate  $C_{p,N}$ , and thus predict the strength and range of the attraction. Because the phase behavior was independent of polymer dispersity, however, the phase behavior of samples featuring short ranged attractions ( $R_g/a < 0.05$ ) can be predicted once  $C_{p,N}$  has been calculated. The independence of phase behavior on polymer size and dispersity may break down for longer-ranged attractions, where the shape of the potential plays a role in the phase behavior, and is an open question for future work. Hence this work suggests that polymers of high

dispersity, which are more affordable than uniformly distributed polymers, can be used for applications requiring certain final structures if all polymers in the distribution are small compared to the particles and if the desired phase behavior is far from non-equilibrium boundaries. It also suggests the ability to tune the final polymer concentration by mixing polymers of different sizes to control particle phase behavior.

## Acknowledgements

Support from the National Science Foundation (CBET-1438204) and the Welch Foundation (E-1869) is gratefully acknowledged. We thank Peter Vekilov for the use of the DLS instrument, Megan Robertson for use of the DHR-2 rheometer, and Jeremy Palmer, Ryan Poling-Skutvik, and Ryan Roberts for helpful discussions.

## References

- 1 S. Asakura and F. Oosawa, *J. Chem. Phys.*, 1954, **22**, 1255–1256.
- 2 S. Asakura and F. Oosawa, *J. Polym. Sci.*, 1958, **33**, 183–192.
- 3 H. N. W. Lekkerkerker, W. C. K. Poon, P. N. Pusey, A. Stroobants and P. B. Warren, *Europhys. Lett.*, 1992, **20**, 559–564.
- 4 H. N. W. Lekkerkerker and R. Tuinier, *Colloids and the depletion interaction*, Springer Netherlands, Dordrecht, 2011.
- 5 K. N. Pham, A. M. Puertas, J. Bergenholtz, S. U. Egelhaaf, A. Moussaïd, P. N. Pusey, A. B. Schofield, M. E. Cates, M. Fuchs and W. C. K. Poon, *Science*, 2002, **296**, 104–106.
- 6 L. J. Kaufman and D. A. Weitz, *J. Chem. Phys.*, 2006, **125**, 074716.
- 7 E. H. A. de Hoog, W. K. Kegels, A. van Blaaderen and H. N. W. Lekkerkerker, *Phys. Rev. E: Stat., Nonlinear, Soft Matter Phys.*, 2001, **64**, 021407.
- 8 J. R. Savage and A. D. Dinsmore, *Phys. Rev. Lett.*, 2009, **102**, 198302.
- 9 S. M. Ilett, A. Orrock, W. C. K. Poon and P. N. Pusey, *Phys. Rev. E: Stat. Phys., Plasmas, Fluids, Relat. Interdiscip. Top.*, 1995, **51**, 1344–1352.
- 10 J. C. Conrad, H. M. Wyss, V. Trappe, S. Manley, K. Miyazaki, L. J. Kaufman, A. B. Schofield, D. R. Reichman and D. A. Weitz, *J. Rheol.*, 2010, **54**, 421–438.
- 11 P. J. Lu, J. C. Conrad, H. M. Wyss, A. B. Schofield and D. A. Weitz, *Phys. Rev. Lett.*, 2006, **96**, 028306.
- 12 A. P. Gast, C. K. Hall and W. B. Russel, *J. Colloid Interface Sci.*, 1983, **96**, 251–267.
- 13 A. P. Gast, W. B. Russel and C. K. Hall, *J. Colloid Interface Sci.*, 1986, **109**, 161–171.
- 14 S. Lim, K. H. Ahn and M. Yamamura, *Langmuir*, 2013, **29**, 8233–8244.
- 15 R. Mafi, C. Gray, R. Pelton, H. Ketelson and J. Davis, *Colloids Surf., B*, 2014, **122**, 7–11.
- 16 D. Marenduzzo, K. Finan and P. R. Cook, *J. Cell Biol.*, 2006, **175**, 681–686.
- 17 M. S. Cheung, D. Klimov and D. Thirumalai, *Proc. Natl. Acad. Sci. U. S. A.*, 2005, **102**, 4753–4758.
- 18 A. P. Minton, *J. Biol. Chem.*, 2001, **276**, 10577–10580.
- 19 S. R. McGuffee and A. H. Elcock, *PLoS Comput. Biol.*, 2010, **6**, e1000694.
- 20 S. Kondrat, O. Zimmermann, W. Wiechert and E. von Lieres, *Phys. Biol.*, 2015, **12**, 046003.
- 21 K. Sozański, F. Ruhnnow, A. Wiśniewska, M. Tabaka, S. Diez and R. Hołyst, *Phys. Rev. Lett.*, 2015, **115**, 218102.
- 22 P. J. Lu, E. Zaccarelli, F. Ciulla, A. B. Schofield, F. Sciortino and D. A. Weitz, *Nature*, 2008, **453**, 499–503.
- 23 S. Ramakrishnan, M. Fuchs, K. S. Schweizer and C. F. Zukoski, *J. Chem. Phys.*, 2002, **116**, 2201–2212.
- 24 R. M. L. Evans, D. J. Fairhurst and W. C. K. Poon, *Phys. Rev. Lett.*, 1998, **81**, 1326–1329.
- 25 M. Fasolo and P. Sollich, *J. Chem. Phys.*, 2005, **122**, 074904.
- 26 B. Ahlström and J. Bergenholtz, *Fluid Phase Equilib.*, 2011, **305**, 9–18.
- 27 T. H. Zhang, B. W. M. Kuipers, W.-D. Tian, J. Groenewold and W. K. Kegels, *Soft Matter*, 2015, **11**, 297–302.
- 28 D. J. Fairhurst, PhD thesis, University of Edinburgh, 1999.
- 29 B. H. Ern e, E. van den Pol, G. J. Vroege, T. Visser and H. H. Wensink, *Langmuir*, 2005, **21**, 1802–1805.
- 30 S. M. Liddle, T. Narayanan and W. C. K. Poon, *J. Phys.: Condens. Matter*, 2011, **23**, 194116.
- 31 R. Pandey and J. C. Conrad, *Phys. Rev. E*, 2016, **93**, 012610.
- 32 N. J. Smith and P. A. Williams, *J. Chem. Soc., Faraday Trans.*, 1995, **91**, 1483–1489.
- 33 M. J. Snowden, S. M. Clegg, P. A. Williams and I. D. Robb, *J. Chem. Soc., Faraday Trans.*, 1991, **87**, 2201–2207.
- 34 R. Tuinier and A. V. Petukhov, *Macromol. Theory Simul.*, 2002, **11**, 975–984.
- 35 J. Y. Walz, *J. Colloid Interface Sci.*, 1996, **178**, 505–513.
- 36 R. P. Sear and D. Frenkel, *Phys. Rev. E: Stat. Phys., Plasmas, Fluids, Relat. Interdiscip. Top.*, 1997, **55**, 1677–1681.
- 37 P. B. Warren, *Langmuir*, 1997, **13**, 4588–4594.
- 38 M. Piech and J. Y. Walz, *J. Colloid Interface Sci.*, 2000, **225**, 134–146.
- 39 P. Bryk and M. Bryk, *J. Colloid Interface Sci.*, 2009, **338**, 92–98.
- 40 D. Goulding and J.-P. Hansen, *Mol. Phys.*, 2001, **99**, 865–874.
- 41 S. Yang, H. Tan, D. Yan, E. Nies and A.-C. Shi, *Phys. Rev. E: Stat., Nonlinear, Soft Matter Phys.*, 2007, **75**, 061803.
- 42 S. Biggs, *Phys. Chem. Chem. Phys.*, 2010, **12**, 4172–4177.
- 43 D. Kleshchanok, R. Tuinier and P. R. Lang, *Langmuir*, 2006, **22**, 9121–9128.
- 44 P. Jenkins and B. Vincent, *Langmuir*, 1996, **12**, 3107–3113.
- 45 J. J. Lietor-Santos, C. Kim, M. L. Lynch, A. Fernandez-Nieves and D. A. Weitz, *Langmuir*, 2010, **26**, 3174–3178.
- 46 J. L. Burns, Y.-d. Yan, G. J. Jameson and S. Biggs, *J. Colloid Interface Sci.*, 2002, **247**, 24–32.
- 47 L. Antl, J. W. Goodwin, R. D. Hill, R. H. Ottewill, S. M. Owens, S. Papworth and J. A. Waters, *Colloids Surf.*, 1986, **17**, 67–78.
- 48 T. Solomon and M. J. Solomon, *J. Chem. Phys.*, 2006, **124**, 134905.

- 49 A. D. Dinsmore, E. R. Weeks, V. Prasad, A. C. Levitt and D. A. Weitz, *Appl. Opt.*, 2001, **40**, 4152–4159.
- 50 M. E. Leunissen, PhD thesis, Universiteit Utrecht, 2007.
- 51 G. N. Smith, J. E. Hallett and J. Eastoe, *Soft Matter*, 2015, **11**, 8029–8041.
- 52 J. C. Crocker and D. G. Grier, *J. Colloid Interface Sci.*, 1996, **179**, 298–310.
- 53 D. Blair and E. Dufresne, The matlab particle tracking code repository, <http://physics.georgetown.edu/matlab/>.
- 54 P. N. Pusey, *J. Phys.*, 1987, **48**, 709–712.
- 55 C. P. Royall, W. C. K. Poon and E. R. Weeks, *Soft Matter*, 2013, **9**, 17–27.
- 56 P. N. Pusey, E. Zaccarelli, C. Valeriani, E. Sanz, W. C. K. Poon and M. E. Cates, *Philos. Trans.: Math., Phys. Eng. Sci.*, 2009, **367**, 4993–5011.
- 57 C. W. J. Beenakker and P. Mazur, *Phys. A*, 1983, **120**, 388–410.
- 58 C. A. Angell, *Science*, 1995, **267**, 1924–1935.
- 59 E. R. Weeks and D. A. Weitz, *Chem. Phys.*, 2002, **284**, 361–367.
- 60 E. Zaccarelli, I. Saika-Voivod, S. V. Buldyrev, A. J. Moreno, P. Tartaglia and F. Sciortino, *J. Chem. Phys.*, 2006, **124**, 124908.
- 61 A. Ochab-Marcinek, S. A. Wieczorek, N. Ziębacz and R. Holyst, *Soft Matter*, 2012, **8**, 11173–11179.
- 62 T.-H. Fan, J. K. G. Dhont and R. Tuinier, *Phys. Rev. E: Stat., Nonlinear, Soft Matter Phys.*, 2007, **75**, 011803.
- 63 T. Kalwarczyk, K. Sozanski, A. Ochab-Marcinek, J. Szymanski, M. Tabaka, S. Hou and R. Holyst, *Adv. Colloid Interface Sci.*, 2015, **223**, 55–63.
- 64 C. J. Dibble, M. Kogan and M. J. Solomon, *Phys. Rev. E: Stat., Nonlinear, Soft Matter Phys.*, 2006, **74**, 041403.
- 65 P. Varadan and M. J. Solomon, *Langmuir*, 2003, **19**, 509–512.
- 66 W. B. Russel, D. A. Saville and W. R. Schowalter, *Colloidal dispersions*, Cambridge University Press, Cambridge, UK, 1991.
- 67 P. G. De Gennes, *C. R. Seances Acad. Sci., Ser. B*, 1979, **288**, 359–361.
- 68 D. Kleshchanok, R. Tuinier and P. R. Lang, *J. Phys.: Condens. Matter*, 2008, **20**, 073101.
- 69 D. Broseta, L. Leibler, A. Lapp and C. Strazielle, *Europhys. Lett.*, 1986, **2**, 733–737.
- 70 M. Fasolo and P. Sollich, *J. Phys.: Condens. Matter*, 2005, **17**, 797–812.
- 71 A. Fortini, M. Dijkstra and R. Tuinier, *J. Phys.: Condens. Matter*, 2005, **17**, 7783–7803.
- 72 C. Gögelein and R. Tuinier, *Eur. Phys. J. E: Soft Matter Biol. Phys.*, 2008, **27**, 171–184.
- 73 J. Zhou, J. S. van Duijneveldt and B. Vincent, *Langmuir*, 2010, **26**, 9397–9402.
- 74 A. Stradner, H. Sedgwick, F. Cardinaux, W. C. K. Poon, S. U. Egelhaaf and P. Schurtenberger, *Nature*, 2004, **432**, 492–495.
- 75 H. Sedgwick, S. U. Egelhaaf and W. C. K. Poon, *J. Phys.: Condens. Matter*, 2004, **16**, S4913–S4922.
- 76 A. I. Campbell, V. J. Anderson, J. S. van Duijneveldt and P. Bartlett, *Phys. Rev. Lett.*, 2005, **94**, 208301.
- 77 J. C. F. Toledano, F. Sciortino and E. Zaccarelli, *Soft Matter*, 2009, **5**, 2390–2398.
- 78 T. H. Zhang, J. Klok, R. H. Tromp, J. Groenewold and W. K. Kegel, *Soft Matter*, 2012, **8**, 667–672.
- 79 M. Kohl, R. F. Capellmann, M. Laurati, S. U. Egelhaaf and M. Schmiedeberg, *Nat. Commun.*, 2016, **7**, 11817.
- 80 M. Spannuth and J. C. Conrad, *Phys. Rev. Lett.*, 2012, **109**, 028301.
- 81 M. G. Noro and D. Frenkel, *J. Chem. Phys.*, 2000, **113**, 2941–2944.
- 82 T. Eckert and E. Bartsch, *Phys. Rev. Lett.*, 2002, **89**, 125701.
- 83 N. Willenbacher, J. S. Vesaratchanon, O. Thorwarth and E. Bartsch, *Soft Matter*, 2011, **7**, 5777–5788.
- 84 J. Hendricks, R. Capellmann, A. B. Schofield, S. U. Egelhaaf and M. Laurati, *Phys. Rev. E: Stat., Nonlinear, Soft Matter Phys.*, 2015, **91**, 032308.
- 85 I. Teraoka, Z. Zhou, K. H. Langley and F. E. Karasz, *Macromolecules*, 1993, **26**, 3223–3226.